Chapter

Morphology Evolution of DF2 (AISI-O1) Surface Micromachined by Pulsed Nd:YAG Laser

Kelvii Wei Guo

Abstract

Pulsed Nd:YAG laser was taken to premicromachine DF2 (AISI-O1) cold work steel. The effect of laser-irradiated parameters on the morphology evolution of the processed surface was investigated by 3D profilometer, atomic force microscope (AFM), scanning electron microscopy (SEM), and optical microscopy (OM). Results show that when DF2 (AISI-O1) specimens were irradiated with various parameters, the morphology of DF2 (AISI-O1) cold work steel was changed correspondingly. Moreover, it demonstrates that for a given laser, various kinds of morphology of a laser-machined surface could be established successfully to satisfy with the desired finish surface for the practical applications later.

Keywords: surface morphology, pulsed Nd:YAG laser, micromachining, DF2 (AISI-O1)

1. Introduction

The quality requirements of the dies and molds are high during the glass, metal, and plastic product fabrication. Small abrasive tools or wheels that can rotate and vibrate by themselves can be used to improve the easily accessible areas of some surface. But, in practical situation, the surface of these molds and dies is mainly finished or processed by the hand. The processing is relied on the successive size decrement of particles taken for abrasion distributed on abrasive papers or cloths in order to make the finished surface meet with the practical applications.

The shortcomings of operators make a lot of limitations in these methods during the manual processing. It should be noted that operators have to be seriously trained to gain the considerable experiment and meet with the requirements of practical operations at various conditions, especially with the small radii equipment to attain the effective application. Moreover, it also requires the consistent and repeatable operation. In addition, it requires a skilled operator to take 10 days to process 10 dies with the complicated forms. Meanwhile, it also needs to make sure that all the finished dies are identical after completion. More importantly, the accuracy of the die dimension is not lost after the finished surface is achieved. Therefore, an operator with high experiences and skills is definitely expensive. It is well known that a well-trained operator is essential to the process of manufacturing.

As mentioned above, it can be seen that it is also extremely tedious and more time-consuming for this process. Research shows that the time consumed on a mold

finishing can be about 37% of the total time of the entire mold production [1]. Consequently, it is crucial and urgent to improve or enhance the quality of die or mold at the final step with the less number of the trained and skilled operators or the decrement of processing time in order to dramatically cut the overall cost.

For the processes with automatic techniques, there are also some limitations to the closed die processing. Research shows that it is very slow for the precision machining by a single-point diamond tool. Moreover, it is not easily available for industrial conditions and hard for the flat surfaces [1–3]. Chemical micromachining and electrochemical micromachining are limited in their application and can be difficult to control [3–6]. Some research has been carried out into the use of robot-controlled finishing tools [1, 3–5, 7–9]. However, the use of a rotary wheel or ultrasonic chisel requires that the micromachined surface should be almost parallel to the axis of the wheel or the chisel angle. It should be noted that it is not suitable for almost flat workpieces and limits its applications.

The ultrasonic machining can be used to achieve the removal of the controllable material [1, 3]. By this technique, the hammering force between the abrasive particles (in water-based slurry) and the workpiece at high frequency can remove the material from the processed surface. As a result, the shapes with the complicated forms can be achieved by the suitably designed tools. Although it is potential for processing the closed molds or dies, there are still some disadvantages, especially for the indentation of workpiece and the drilling of the fixed location.

Currently, it is efficient and successful to apply the abrasive flow machining to process the open molds or dies. In this process, a mix of abrasive particles is taken to finish the surface by hydraulic power in the form of suspension in a pliable polymer base. However, limitation is still to restrict this process from finishing the molds or dies without an exit and an entry for the flowing mix in the hollow or tubular form [1, 2].

To date, laser has been widely used as a machine tool to modify the surface of the engineering materials, such as laser surface alloying, laser cladding, surface texturing, laser physical vapor deposition, etc. [1, 3–5]. Recently, micromachining by laser technique is gaining more attention to be an interesting method to machine lens, diamonds, etc. [7–12].

On the basis of the abovementioned, an investigation has been taken to micromachine DF2 steel with the excellent non-contact possibility and the unique characteristics of Nd:YAG laser radiation.

2. Experimental material and procedures

2.1 Experimental material

The chemical composition of DF2 cold work steel is shown in **Table 1**.

2.2 Experimental procedures

The materials were machined into 25 × 10 × 10 mm and carefully cleaned by acetone and pure ethyl alcohol to remove any contaminants on its surface. **Figure 1**

Element	C	Si	Mn	Cr	W	V	Fe
(wt.%)	0.9	0.3	1.2	0.5	0.5	0.1	Bal.

Table 1.
Chemical composition of DF2 (AISI-O1) cold work steel.

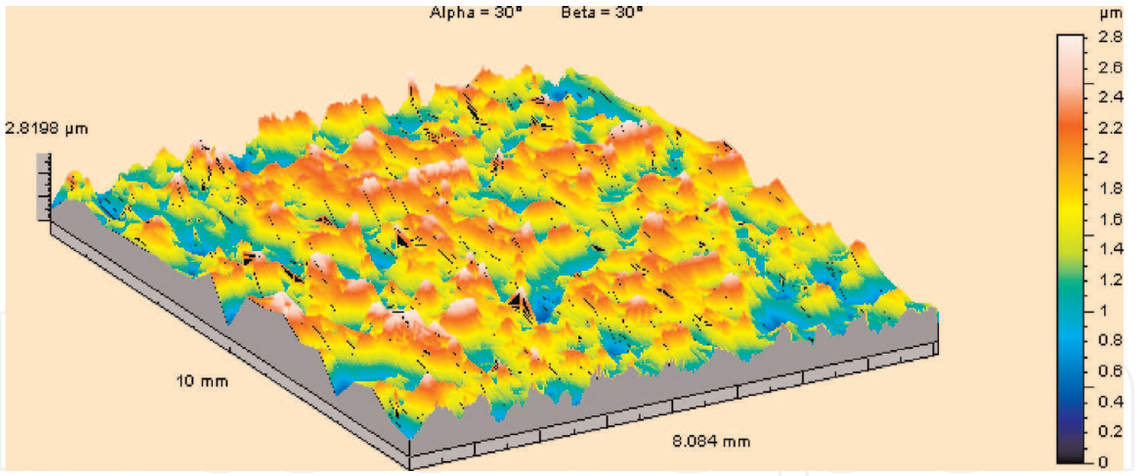

Figure 1.
Initial topographies of specimens Ra = 0.4 µm.

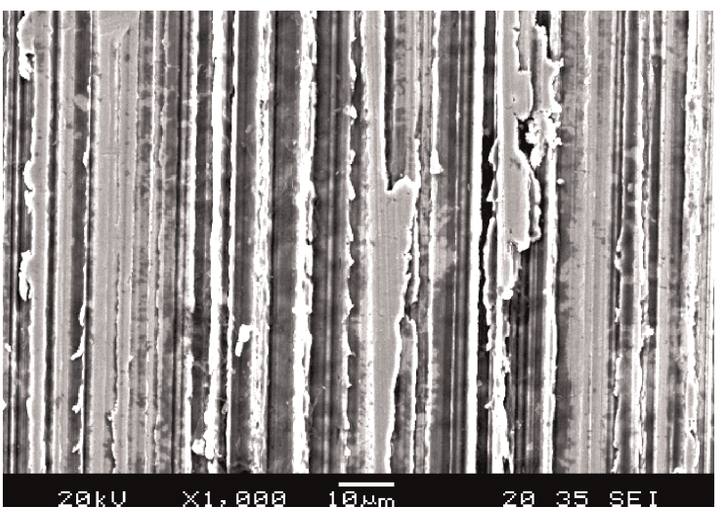

Figure 2.
SEM of the DF2 (AISI-O1) initial surfaces.

Figure 3.
Microstructure of DF2 (AISI-O1) steel.

shows the Talysurf 3D topography of the original DF2 tool steel specimens categorized with the initially machined surface roughness *R*a = 0.4 μm, while **Figure 2** shows the corresponding 2D SEM morphology. The microstructure of DF2 steel is shown in **Figure 3**.

A GSI Lumonics Model JK702H pulsed Nd:YAG TEM_{00} mode laser system, with wavelength of 1.06 μm, defocused distance of 15 mm, and focus spot diameter of ~1.26 mm on the substrate surface, was used to irradiate the DF2 steel.

After being processed, the surface morphology was observed by atomic force microscope (AFM), Taylor Hobson profilometer/Talysurf PGI, and scanning electron microscope (SEM) JEOL/JSM-5600.

3. Results and discussion

3.1 Influence of laser scanning speed (feedrate)

Comparing **Figure 1** with **Figure 4**, if the parameters are not set properly, the surface will be rather roughened than smoothened though most of the high plateaus are removed from the initial specimen surface. The initial surface with the surface roughness of 0.4 μm was irradiated with laser pulse frequency of 25 Hz, pulse energy of 1 J, and pulse duration of 3 ms. Results are shown in **Figure 4**. It suggests that when the feedrate is 300 mm/min, the achieved 3D topography of the irradiated surface is the smoothest. It also shows that with the variation of laser feedrates, the irradiated surface changed correspondingly. During the period of between 100 and 300 mm/min, the irradiated surface is becoming more and more smoother. However, when the feedrate is higher than 300 mm/min, the quality of the irradiated surface will be coarser. **Figure 4a–c** illustrates the 3D morphology of the improved smoothness of processed surface with the laser feedrate of <300 mm/min, and **Figure 4c** and **d** shows 3D morphology of unsmooth processed surface with the laser feedrate higher than 300 mm/min.

The relationship between the laser feedrate (scanning speed) and the roughness of the processed surface is shown in **Figure 5**. It indicates that when the laser scanning speed increases, the roughness of the processed surface will be decreased correspondingly. Moreover, when the laser scanning speed is up to 300 mm/min, the roughness of the processed surface is at its minimum. After that, with the laser scanning speed increasing further, the roughness of the processed surface will be increased again. Moreover, the roughness of the processed surface is generally higher than the initial condition when the relative feedrate is below 300 mm/min. However, it decreases with the increase in the relative feedrate. When the relative feedrate is at 400 mm/min, the irradiated roughness is increased to some level.

3.2 Effect of pulse energy of laser irradiating

According to the abovementioned study, the laser scanning speed is taken as 300 mm/min in the subsequent tests as the optimal feedrate. The relationship between the roughness of the processed surface and the laser irradiating energy is shown in **Figure 6**. It is well known that if the laser pulse energy raises, the energy interaction between the workpiece and laser will be raised simultaneously. When the laser pulse energy is so high, the energy input into the workpiece will be enhanced. As a result, the surface of the workpiece will be melted and the roughness of the processed surface will change seriously, especially for deteriorating the mechanical properties of the processed workpiece in the subsequent practical application afterward. **Figure 7** shows the relationship between the roughness of the

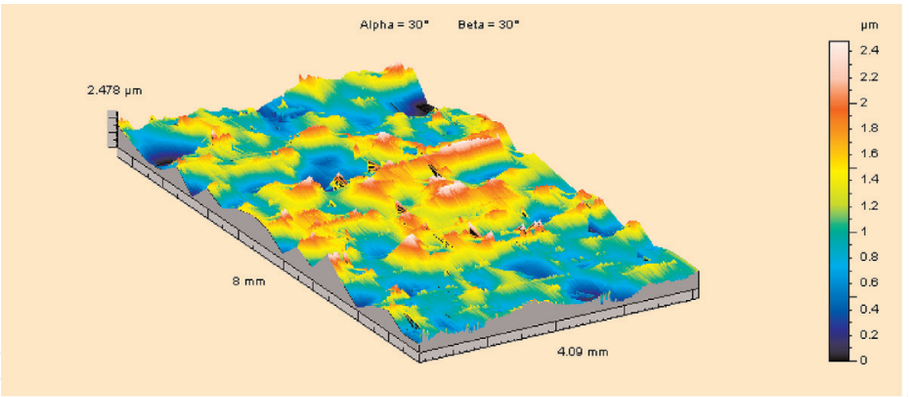

(a)

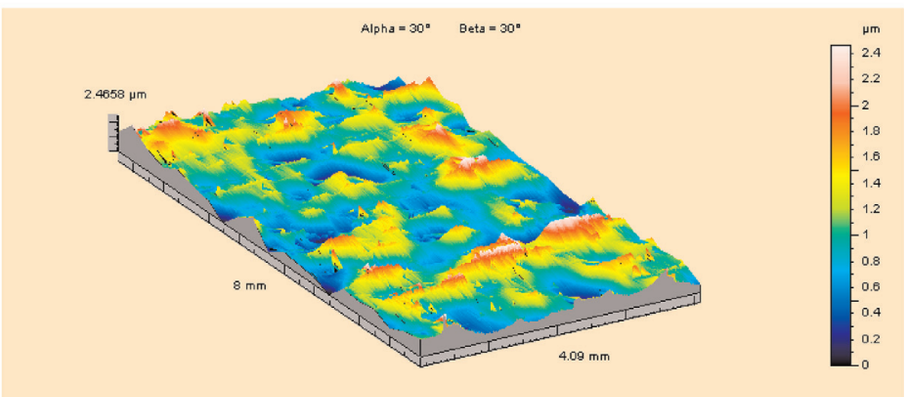

(b)

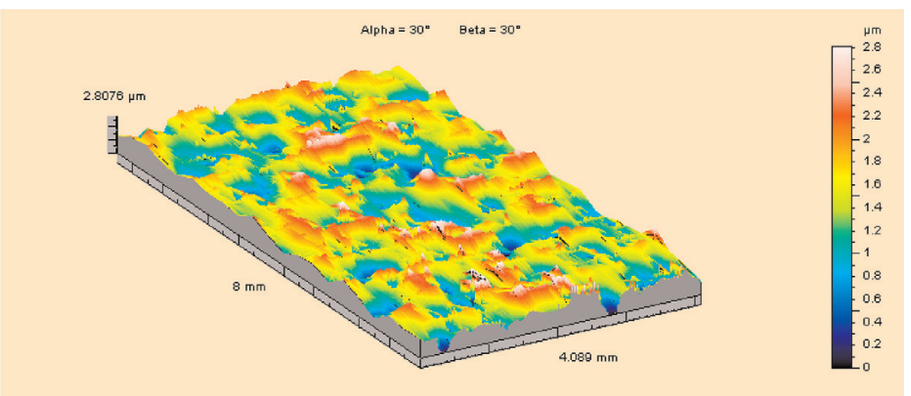

(c)

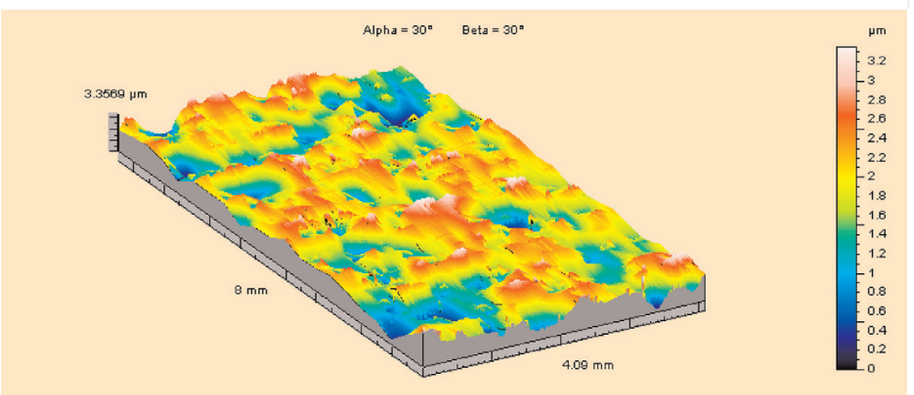

(d)

Figure 4.
Surface textures of laser micromachining at various feedrates. (a) 400 mm/min, (b) 300 mm/min, (c) 200 mm/min, and (d) 100 mm/min. Pulse energy = 1 J, f = 25 Hz, PD = 3 ms.

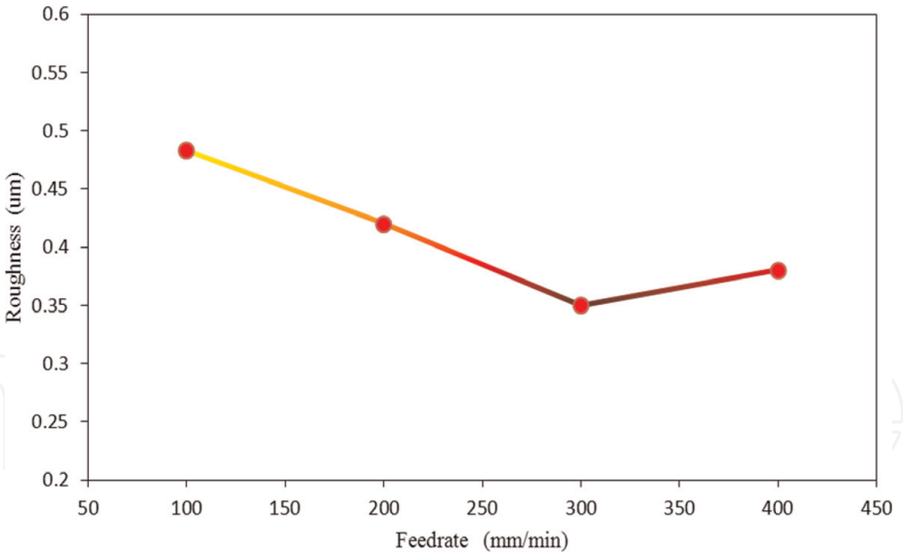

Figure 5.
Relationship between surface roughness and feedrate.

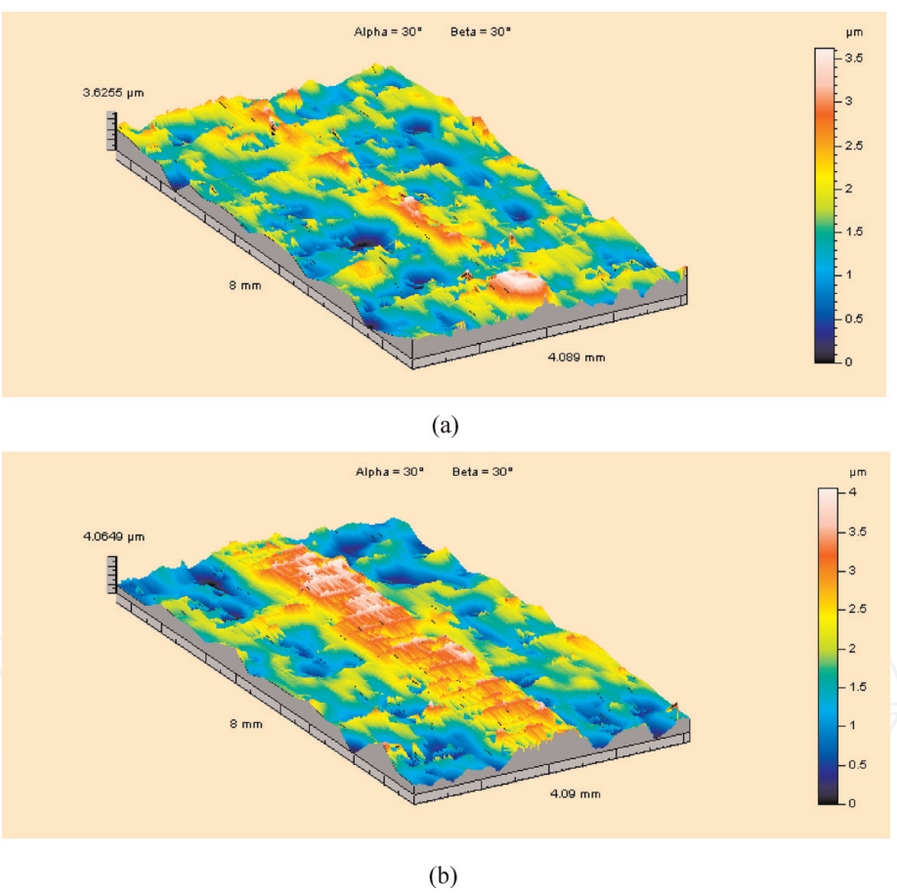

Figure 6.
Surface textures of laser micromachining at various pulse energies. (a) Pulse energy = 2 J and (b) pulse energy = 3 J. Feedrate = 300 mm/min, f = 25 Hz, PD = 3 ms.

processed surface and laser pulse energy. Results indicate that the roughness variation of the processed surface is correlated with the laser pulse energy. It expresses that when the laser pulse energy is 2 J, the roughness of the processed surface is 0.49 μm with some protrusions distributed on the surface as shown in **Figure 6a**. With the laser pulse energy increasing, more protrusions are scattered on the processed surface. Consequently, the roughness of the processed surface is up to 0.7 μm. Meanwhile, the laser-affected zone is becoming wider and larger as shown

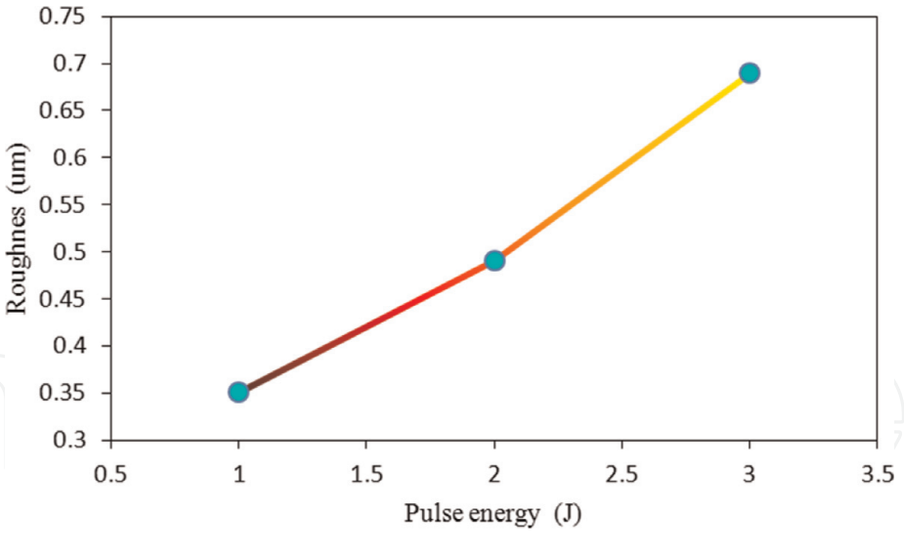

Figure 7.
Relationship between surface roughness and pulse energy.

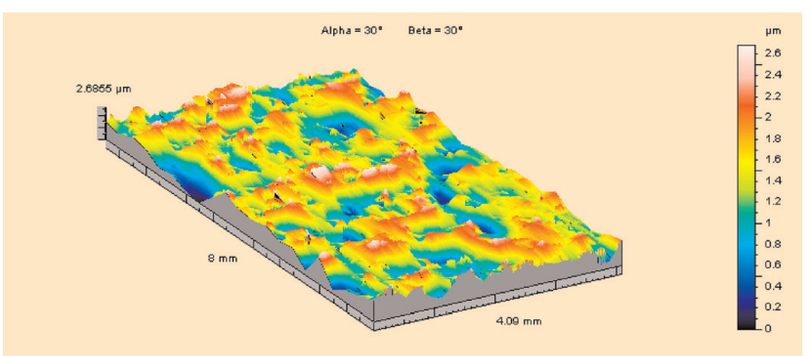

(a)

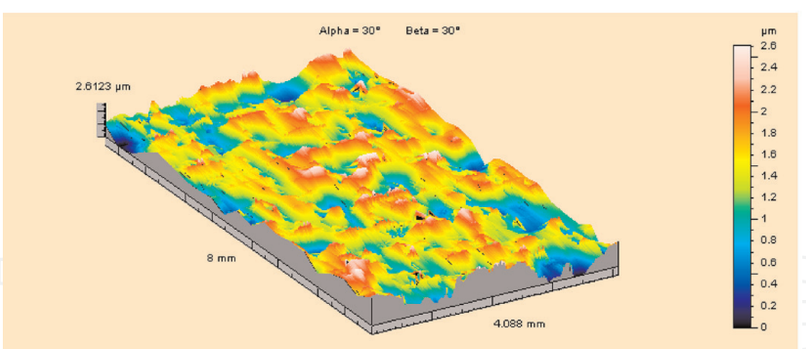

(b)

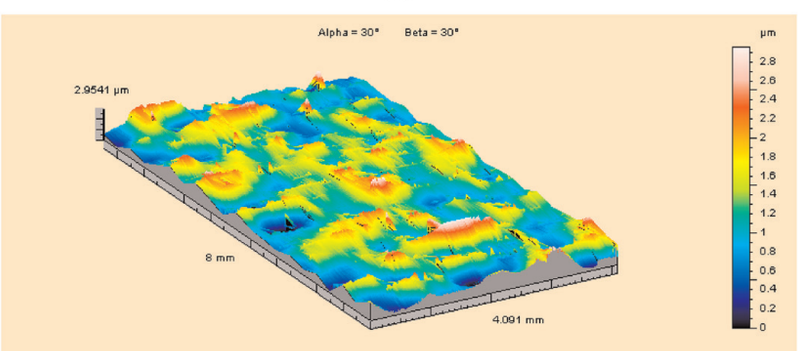

(c)

Figure 8.
Surface textures of laser micromachining at various pulse frequencies. (a) f = 15 Hz, (b) f = 20 Hz, (c) f = 30 Hz. Pulse energy = 1 J, feedrate = 300 mm/min, PD = 3 ms.

in **Figure 6b**, which indicates that if laser pulse energy is equal to or higher than 2 J, the results of the final processed surface is generally not acceptable.

3.3 Influence of laser irradiation frequency (repetition rate)

Figure 8 shows the laser-irradiated surface scanned at various pulse frequencies. It shows that the roughness of the irradiated surface decreases with the pulse frequency increasing. However, at a pulse frequency of 30 Hz, the roughness of the processed surface is distinctively higher again resulting in a coarser finished surface. Its corresponding roughness of the processed surface varied with the laser pulse energy shown in **Figure 9**. Results illustrate that when the laser pulse energy varies from 20 to 25 Hz, the roughness of the processed surface is <0.4 μm, and the processed surface is smoother at the optimal level. However, the roughness of the processed surface will be increased obviously in the case the laser pulse frequency increases, e.g., 30 Hz.

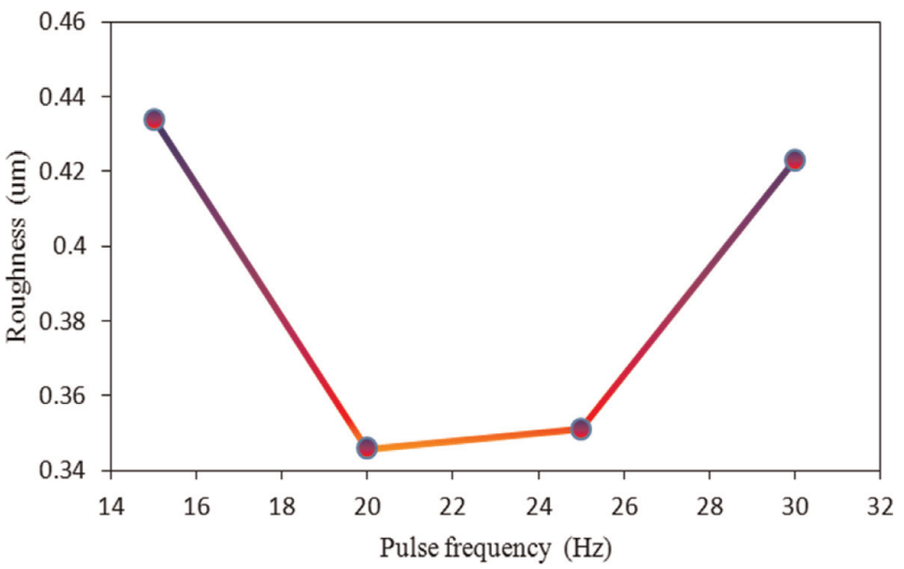

Figure 9.
Relationship between surface roughness and pulse frequencies.

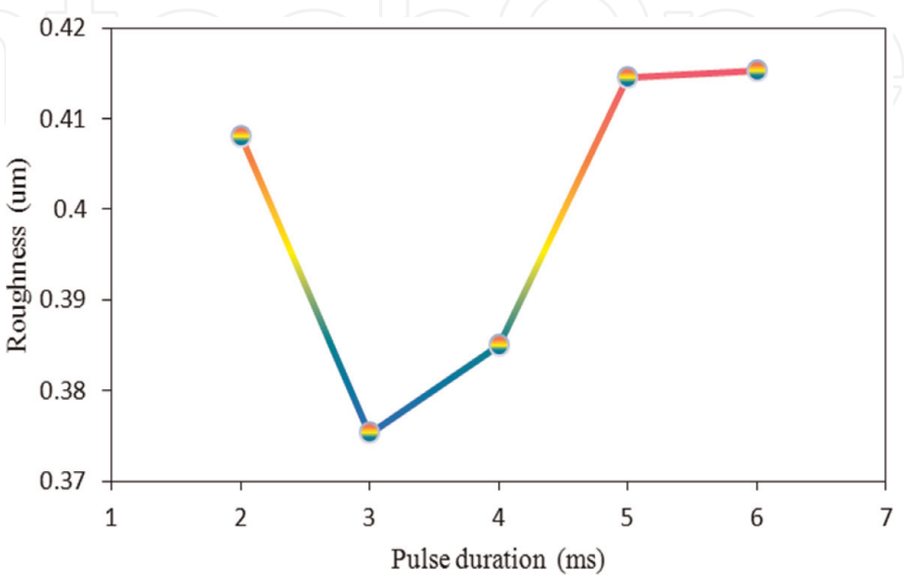

Figure 10.
Relationship between surface roughness and pulse duration.

3.4 Influence of laser micromachining pulse duration (PD)

Figure 10 shows the relationship between the laser pulse duration and the roughness of the processed surface. Results elucidate that when the laser pulse duration is decreased, the roughness of the processed surface will be decreased correspondingly. It also shows that the roughness of the processed surface is at its minimum when the laser pulse duration is 3 ms. With the decrement of the laser pulse duration further (e.g., 2 ms), the roughness of the processed surface will be increased remarkably. In addition, the roughness of the processed surface will be coarser when the laser pulse duration exceeds 4 ms.

4. Discussions

4.1 Influence of feedrate and pulse frequency

As the irradiation path of a continuous scanning mode using a pulsed laser with pulse duration PD and frequency f is essentially consisted of a series of overlapping spots (**Figure 11**), the basic condition to realize the micromachining by a pulsed laser is that two successive spots in a continuous scanning mode should be tangential to each other, viz.:

$$0 < \delta \leq D \tag{1}$$

where D is the laser spot diameter, δ is the distance of one pulse, δ_1 is the distance with the laser-on duration, and δ_2 is the distance with the laser-off duration, and it is defined as

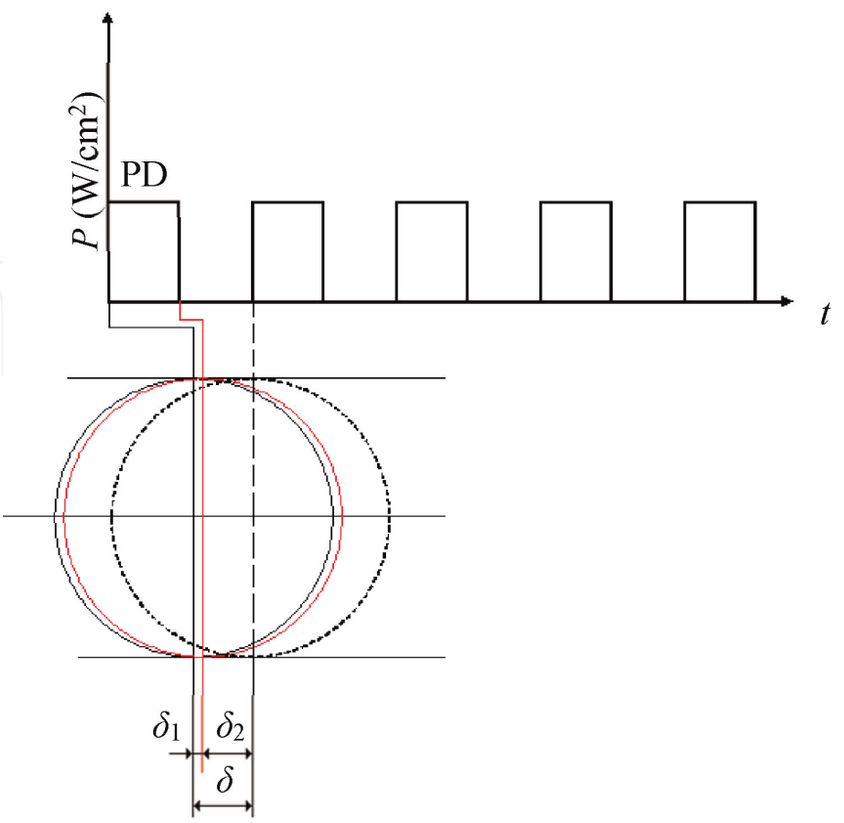

Figure 11.
Schematic image of a laser pulse irradiated on the surface.

$$\delta = \frac{Feedrate}{f} \tag{2}$$

Substituting Eq. (2) into Eq. (1) subsequently gives

$$0 < \frac{Feedrate}{f} \leq D \tag{3}$$

which can then be expressed as

$$0 < Feedrate \leq Df \tag{4}$$

Figure 12 shows the relationship between δ and pulse frequency f (see Eq. (2)) at various feedrates and its corresponding percentage of overlapping of two successive laser pulses in the continuous scanning mode. It shows that the laser frequency increased (i) with the decrease of δ (see the solid lines in **Figure 12**) and (ii) simultaneously with the increase in the overlap percentage (see the dashed lines in **Figure 12**). When the feedrate is at 300 mm/min, the pulse frequency of 20–25 Hz leads to the δ about 0.25–0.20 mm and the overlap percentage about 60–68%.

Under the conditions of the experimental feedrates and pulse frequencies in this study, the distances of a single laser pulse (δ) are thus smaller than the laser spot diameter (D), which meets the constraint of Eq. (1) for the realization of laser micromachining phenomenon. The mechanisms involved in achieving the micromachining effect at the operational parameters of pulse frequency f = 20–25 Hz and feedrate = 300 mm/min need to be explored.

In view of the overlapping geometry of the irradiation spot under continuous scanning mode, the laser micromachining process is in quasi-steady state (**Figure 13**) when the moving distance of the spot within a single pulse is equal to or greater than the spot diameter. The solid lines with different colors in **Figure 13** present the laser spot during the "on"-duration (δ_1 in **Figure 11**) of a PD, while their individual counterpart dashed lines, respectively, stand for the shifting of the laser

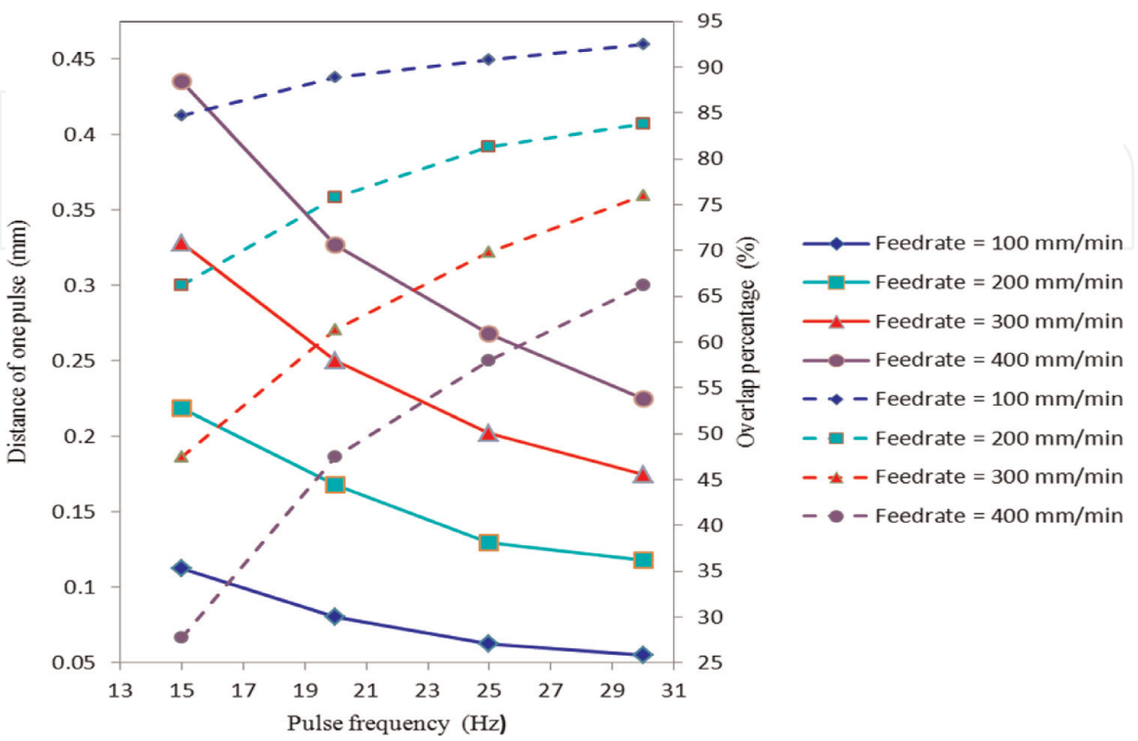

Figure 12.
Relationship between δ and pulse frequency at various feedrates.

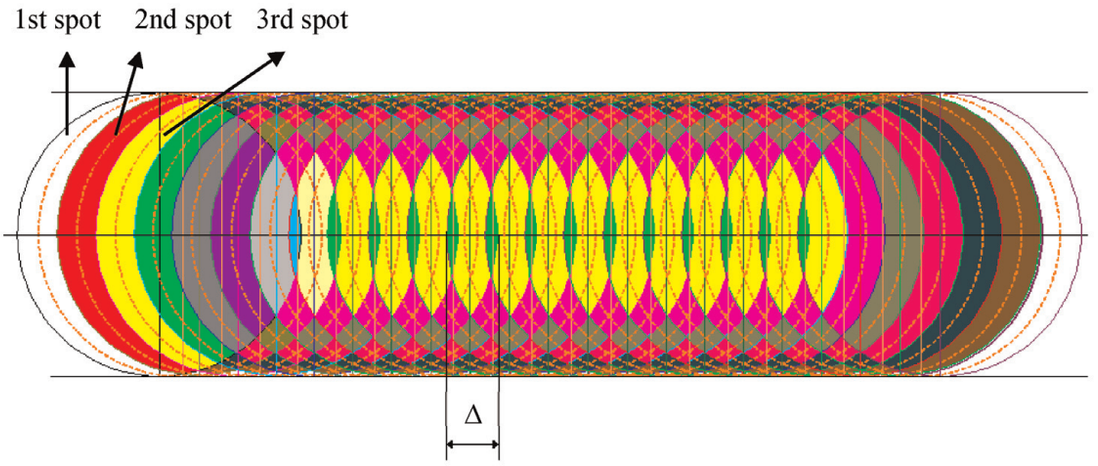

Figure 13.
Schematic diagram of laser micromachining.

spot during the "off"-duration (δ_2 in **Figure 11**) of the PD. The areas filled with various colors in **Figure 13** stand for the level of different overlapping (typically: the area in red color stands for the occurrence of only one overlap; the area in light yellow stands for the occurrence of two overlapped, and so on). Let Δ be the effective micromachining size along the central line; it can then be expressed as

$$\Delta = D - \left\| \frac{D}{\delta} \right\| \times \delta + \delta \tag{5}$$

Figure 14 shows the behaviors of effective overlap percentage versus pulse frequency at the experimental feedrates. It shows that the relative overlap percentage for the feedrate = 300 mm/min is lower than that of other feedrates when the pulse frequency is at and beyond 20 Hz. When the pulse frequency is below 20 Hz, the effective overlap percentage is increased distinctly with the decrease in pulse frequency. Experimentally, irradiated specimens with smaller overlap percentage seemed to give better metallurgical aspect. This suggests that the surface can be micromachined successfully according to various feedrates and pulse frequencies. When the effective overlap percentage inclined to null, the laser micromachining

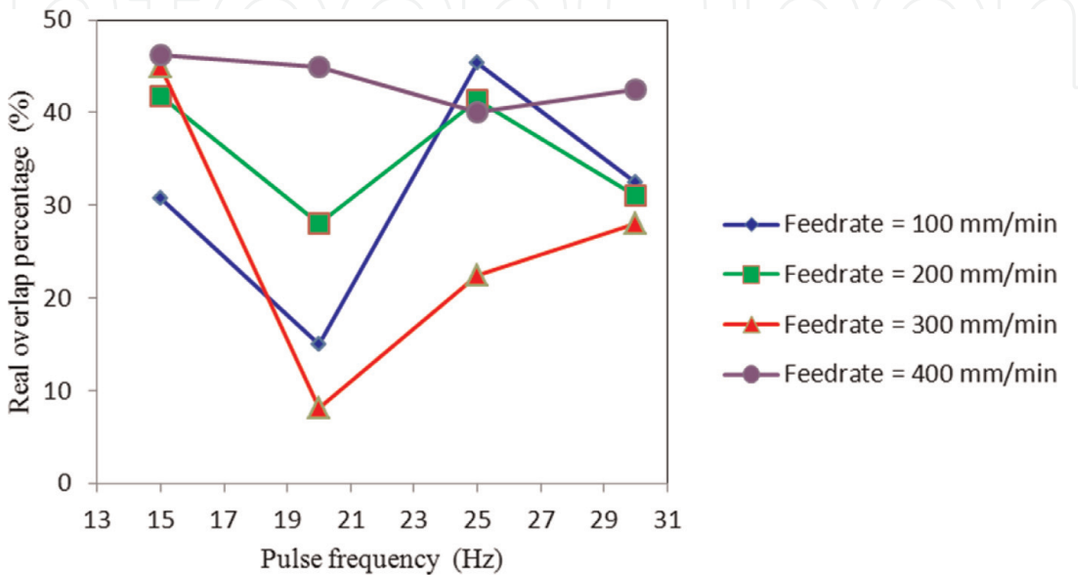

Figure 14.
Effective overlapping percentage versus pulse frequency at various feedrates.

will be of the ideal conditions as generated by a single spot irradiation. Under such conditions, it gives

$$\left\| \frac{D}{\delta} \right\| = 0 \tag{6}$$

Subsequently, substituting Eq. (2) into Eq. (6) gives

$$\left\| \frac{D \times f}{Feedrate} \right\| = 0 \tag{7}$$

Taking D = 1.26 mm, Eq. (7) is therefore transformed into

$$126 \times f = 100 \times n \times Feedrate(f, n = 1, 2, 3) \tag{8}$$

in which n stands for numbers of macroscopical overlaps. When n is equal to 1, the two continuous laser spots are tangential to each other, implying both macroscopical overlap percentage and effective overlap percentage are equal to 0. When f is 20 Hz and feedrate is 300 mm/min, it can be deduced that the value of n is therefore 5 that subsequently leads to 80% (4/5) macroscopical overlap percentage and 20% (1/5) effective overlap percentage. When f is 20 Hz, the ideal feedrate is thus estimated as $\frac{126 \times 20}{5 \times 100} \times 60 = 302.4$ mm/min that is very close to 300 mm/min. This is the reason why the texture of the micromachined surface is better when the laser is set at pulse frequency of 20 Hz and feedrate of 300 mm/min.

4.2 Influence of laser pulse energy and pulse duration (PD)

4.2.1 Physical model of laser micromachining

Figure 15 shows the physical model of Nd:YAG pulsed laser micromachining a specimen along its X-axial direction with certain specific feedrate.

4.2.2 Temperature field of laser micromachining

Figure 16 shows the model with a point source irradiating on a heavy substrate; the assumption of instantaneously releasing the laser energy on the surface of a substrate at time t = 0 leads to a temperature rise in the material (point P) as [13]

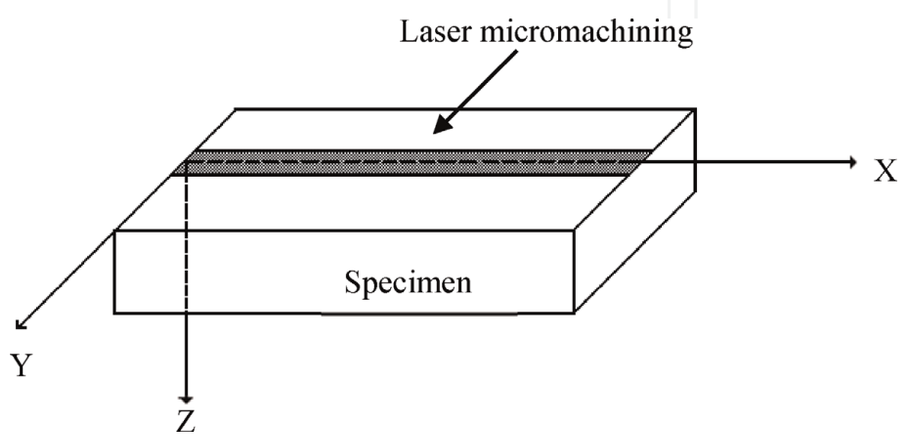

Figure 15.
Schematic diagram of laser micromachining process.

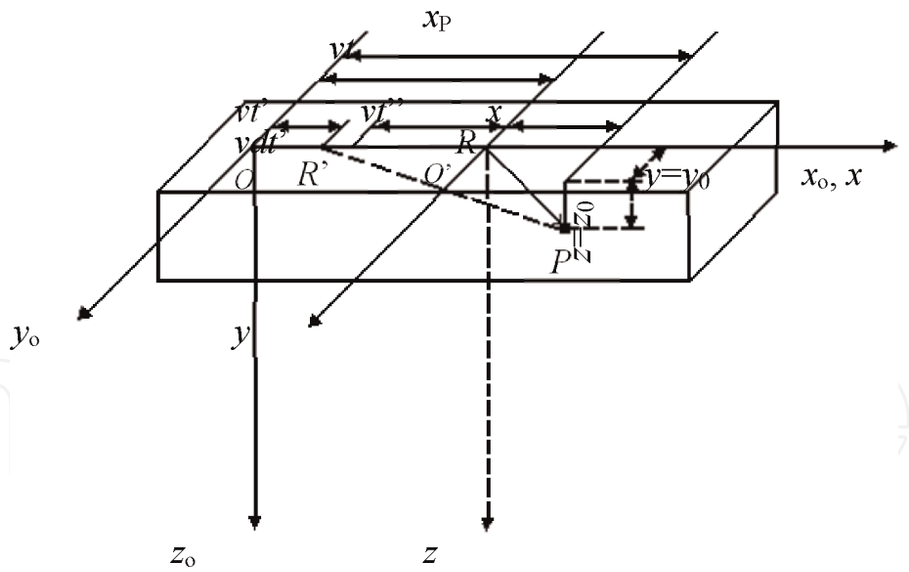

Figure 16.
Moving point source on a semi-infinite substrate.

$$T - T_0 = \frac{Q}{\rho c(4\pi\alpha t)^{\frac{3}{2}}} \exp\left(\frac{-R^2}{4\alpha t}\right) \tag{9}$$

where ρ is the material density, C is specific heat, α is thermal diffusivity, and Q is the input energy. Let the initial temperature, at time $t = 0$, of the generally thick plate be T_0, and the point source of constant power q_0 moves in the x-direction at a constant speed (feedrate) v from the position O.

Within a very short interval from time t' to $t' + dt'$, the amount of heat released at the surface is $dQ = q_o dt'$. By Eq. (9), it produces an infinitesimal temperature rise for point P at time t as

$$dT = \frac{2q_o dt'}{\rho c(4\pi\alpha(t-t'))^{\frac{3}{2}}} \exp\left(-\frac{(R')^2}{4\alpha(t-t')}\right) \tag{10}$$

By defining $t'' = t - t'$, Eq. (10) is thus transformed into

$$dT = \frac{-2q_o dt''}{\rho c(4\pi\alpha t'')^{\frac{3}{2}}} \exp\left(-\frac{(R')^2}{4\alpha t''}\right) \tag{11}$$

Geometrically, **Figure 16** allows $R' = \sqrt{(x_o - vt')^2 + {y_o}^2 + {z_o}^2}$ to be expressed. Subsequently, the transforming of the coordinate system from O to O': $y = y_o$, $z = z_o$, $x = x_o - vt$, and $x_o - vt' = x + vt - vt' = x + vt''$ allows the following expression to be obtained:

$$\begin{aligned} dT &= \frac{-2q_o dt''}{\rho c(4\pi\alpha t'')^{\frac{3}{2}}} \exp\left(-\frac{\left((x+vt'')^2 + y^2 + z^2\right)}{4\alpha t''}\right) \\ &= \frac{-2q_o dt''}{\rho c(4\pi\alpha t'')^{\frac{3}{2}}} \exp\left(-\frac{vx}{2\alpha} - \frac{R^2}{4\alpha t''} - \frac{v^2 t''}{4\alpha}\right) \end{aligned} \tag{12}$$

where $R = \sqrt{x^2 + y^2 + z^2}$.

When temperature distribution is quasi-steady state, Eq. (12) can be expressed as

$$T - T_o = \frac{q_o}{2\pi\rho c\alpha R} \exp\left(-\frac{v}{2\alpha}(R + x)\right) \tag{13}$$

where $q_0 = \eta(N(f, v,)) \times \frac{P}{\frac{\pi D^2}{4} \times PD} = \eta(N(f, v,)) \times \frac{4P}{\pi D^2 \times PD}$ in which $\eta(N(f, v,))$ is the coefficient of laser micromachining input energy and is directly proportional to either the numbers of macroscopical overlaps or the pulse frequency and feedrate. Hence, Eq. (13) can be expressed as

$$T - T_o = \frac{2 \times \eta(N(f, v,)) \times P}{\pi^2 D^2 \rho c\alpha R \times PD} \exp\left(-\frac{v}{2\alpha}(R + x)\right) \tag{14}$$

Define $\xi = \frac{1}{2\pi\rho c\alpha}$, and then Eq. (14) can be written as

$$T - T_o = \frac{\xi \times \eta(N(f, v,)) \times P}{\frac{\pi D^2}{4} \times PD \times R} \exp\left(-\frac{v}{2\alpha}(R + x)\right) \tag{15}$$

Equation (15) expresses the relationship between the laser micromachining temperature and the processing parameters like pulse energy, pulse duration, pulse frequency, and scanning speed (feedrate). The equation indicates that the increase in pulse energy and pulse frequency generally raises the micromachining temperature up. However, the increase in pulse duration and scanning speed (feedrate) accompanies with the decrease in micromachining temperature, while the increase in velocity leads to the decrease in numbers of overlaps under the constant pulse frequency condition, implying a synchronous decrease in $\eta(N)$ and micromachining temperature. Scanning speed (feedrate) is generally having more remarkable impact on the micromachining temperature than the other parameters. At a particular feedrate, there tends to have a threshold of pulse energy, pulse duration, and pulse frequency for laser micromachining successfully. Let us define

$$q = \frac{P}{\frac{\pi D^2}{4} \times PD}, \tag{16}$$

Equation (15) can then be written as

$$T - T_o = \frac{\xi \times \eta(N(f, v,)) \times q}{R} \exp\left(-\frac{v}{2\alpha}(R + x)\right) \tag{17}$$

4.3 Morphology of laser micromachining DF2 (AISI-O1) surface

On the basis of Eq. 17, it shows that the temperature of laser processing is relied on various parameters, such as laser input energy, laser feedrate (scanning speed), laser pulse duration, laser pulse frequency, the properties of the processed materials, and so on. For example, for a certain laser processing temperature, the laser scanning speed (feedrate) is correlated with the input energy of laser processing. In other words, the scanning speed (feedrate) of laser processing should be increased simultaneously with the increment of the input energy of laser processing, and vice versa. In the viewpoint of enhancing or heightening the laser processing efficiently, lowing the input energy of the laser processing or increasing the scanning speed (feedrate) must be taken to minimize the laser-affected zone on the substrate and

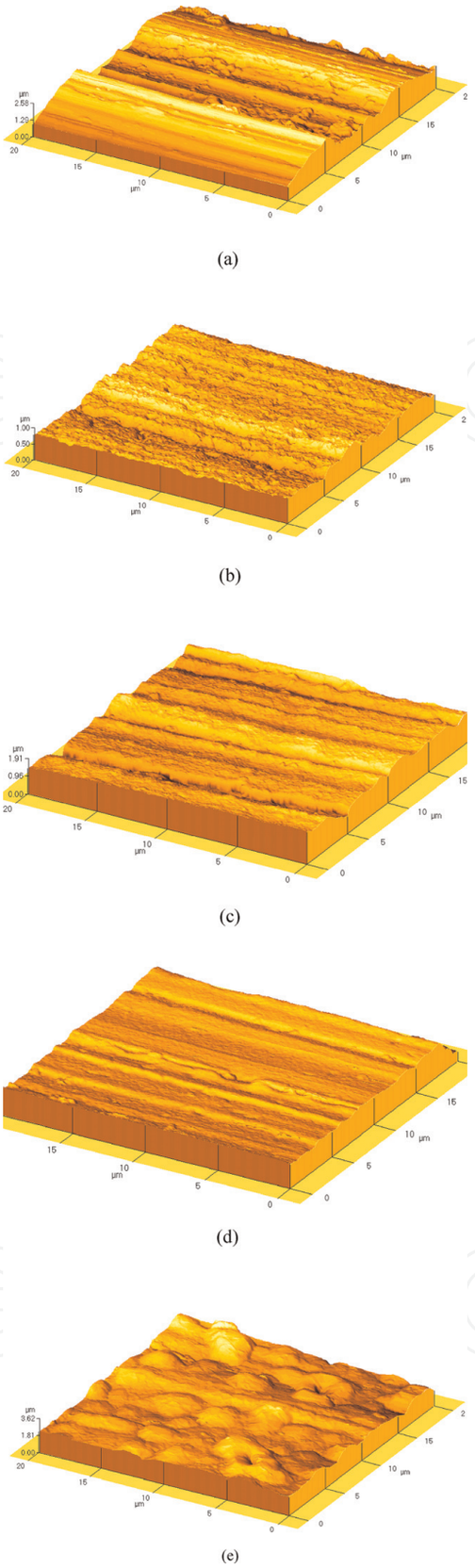

Figure 17.
Three-dimensional morphologies of laser-micromachined surface. (a) Laser-micromachined DF2 (AISI-O1) steel with lower input energy. Processing parameters: v (feedrate) = 400 mm/min, P = 1 J, PD = 2 ms, f = 15 Hz; (b) laser-micromachined DF2 (AISI-O1) steel with higher input energy than (a) processing parameters: v (feedrate) = 300 mm/min, P = 1 J, PD = 3 ms, f = 20 Hz; (c) laser-micromachined DF2 (AISI-O1) steel with medium input energy. Processing parameters: v (feedrate) = 400 mm/min, P = 2 J, PD = 3 ms, f = 20 Hz; (d) laser-micromachined DF2 (AISI-O1) steel with higher input energy than (c). Processing parameters: v (feedrate) = 200 mm/min, P = 2 J, PD = 4 ms, f = 25 Hz and (e) laser-micromachined DF2 (AISI-O1) steel with more higher input energy. Processing parameters: v (feedrate) = 100 mm/min, P = 3 J, PD = 4 ms, f = 30 Hz.

save the source of energy. The three-dimensional morphologies of the laser-micromachined surface with various input energy measured by AFM were shown in **Figure 17**.

Figure 17 shows that the morphology of laser-micromachined surface is changed with laser input energy. When the input energy is lower, the effect of laser processing parameters on the morphology of DF2 is not distinct, as shown in **Figure 17a**. With the increase of input energy, there are large amount of micro-pits distributed on the micromachined surface (**Figure 17b**) which could efficiently improve the load-carrying capacity and permit ease of release for mold made by DF2 [14]. Also, for the surface material removal, the main mechanism of the laser-processed surface relies on evaporation, melting, and its subsequent re-solidification. When the input energy of laser processing is lower, the influence of laser micromachining in this stage will mainly depend on the substrate melting. If the input energy of laser-processed surface of substrate is higher than that shown in **Figure 17b**, the 3D topography of the processed surface will vary accordingly. The relevant results are shown in **Figure 17c**. It shows that the micro-pits distributed on the processed surface as shown in **Figure 17b** are mostly melted and the morphology of the processed surface becomes relatively smooth. The effect of laser micromachining in this period is the synergetic action of the melting and little vaporizing of the substrate. With the input energy becoming higher, the morphology of laser processing will lie on the metal melting and medium vaporizing as shown in **Figure 17d**. It could be found that the surface is covered by melted metal with smoother texture and the property of substrate is changed to some extent because there are more laser energy inputs into the substrate. With the further increase of the input energy into the substrate, the surface of DF2 steel will be melted and vaporized seriously as shown in **Figure 17e**. It can be seen that there are

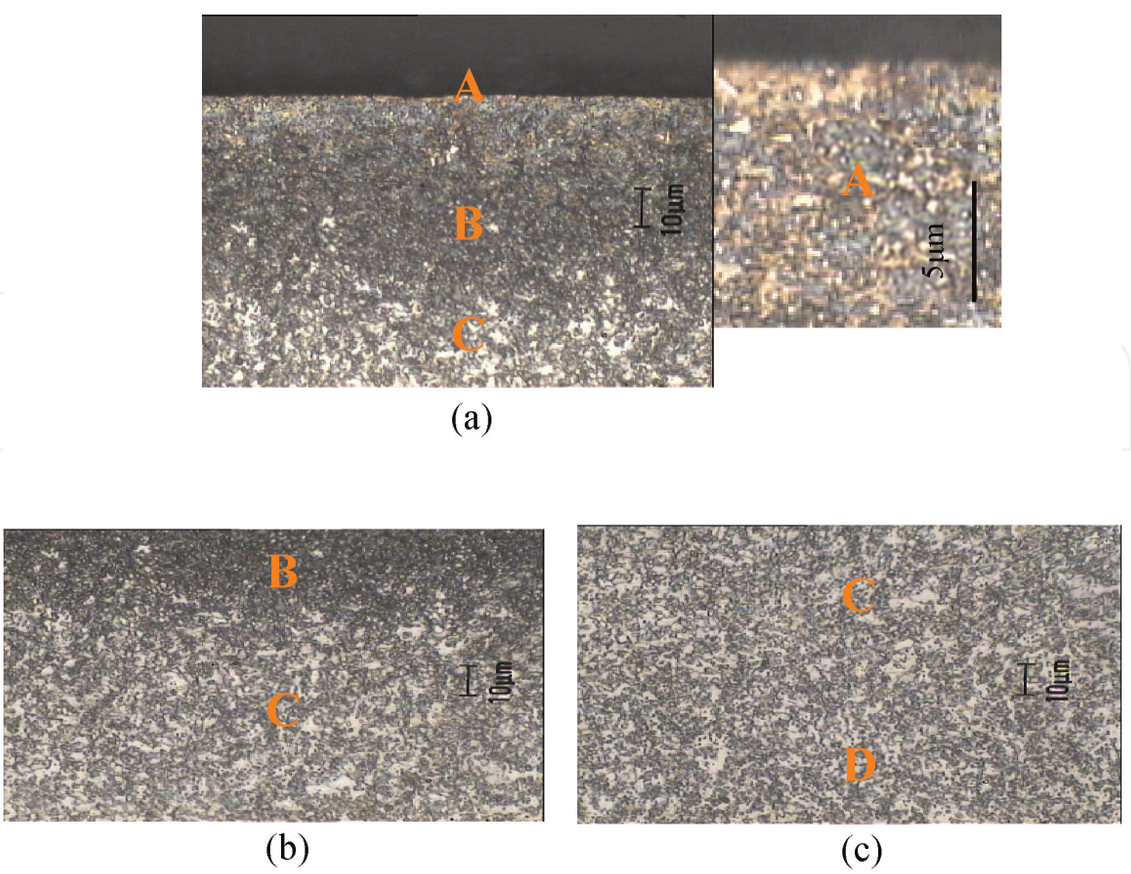

Figure 18.
Cross-section microstructures of laser-micromachined specimen (a) A-Harden layer, B-Fine grained zone, C-Heat affected zone, (b) B-Fine grained zone, C-Heat affected zone, (c) C-Heat affected zone, D-Substrate.

lots of cracks, craters, and protuberances on the processed surface resulting in coarser surface texture, which led to the poor properties of surface. It illustrates that the surface of DF2 steel could be processed successfully under the controlled input energy.

4.4 Microstructure of laser micromachining

Figure 18 shows the cross-section micrograph of laser-micromachined specimen. Obviously, the processed substrate is altered and can be detected directly. The smoother processed surface is achieved by laser micromachining with the microstructure variation as shown in **Figure 18a** labeled as zone A. Zone A, known as the hardened layer, distributes certainly enlarged and spheroidized carbide particles (high magnification in **Figure 18a**). Compared with **Figure 18a** and **b**, there are finer spheroidized carbide particles distributed in the matrix of ferrite as shown in zone B. Consequently, the property of the processed surface of the mold or die is improved to meet well with the practical applications. The heat-affected zone (HAZ), zone C, is shown in **Figure 18b** and **c**. The microstructure of the substrate, zone D, is shown in **Figure 18c**. Comparing **Figure 18c** with **Figure 3**, the microstructure does not change and keeps the same. Furthermore, the microstructure shown in zone C is almost the same as that shown in zone D, which means the energy input into the substrate by laser micromachining is too low to effectively change the mechanical property of materials. Additionally, the average thickness of zone A and zone B is ~40 μm as shown in **Figure 18a**, while the average thickness of zone A is about 10 μm. As a result, the machined surface is suitable for microindustry application.

5. Conclusions

1. DF2 (AISI-O1) cold work steel could be successfully micromachined by pulsed Nd:YAG laser. The optimum laser micromachining parameters achieved by experiments are P = 1 J, feedrate = 300–400 mm/min, PD = 3–4 ms, and f = 20–25 Hz.

2. According to the onset of laser processing temperature, $T - T_o = \frac{\xi \times \eta(N(f,v)) \times q}{R} \exp\left(-\frac{v}{2\alpha}(R+x)\right)$, morphologies of the laser-irradiated surface can be controlled with the relevant processing parameters which is attractive and beneficial to the practical applications in the micromachining world.

Author details

Kelvii Wei Guo
Department of Mechanical and Biomedical Engineering, City University of Hong Kong, Kowloon, Hong Kong

*Address all correspondence to: kelviiguo@yahoo.com

References

[1] Steen WM. Laser Material Processing. 3rd ed. London: Springer-Verlag; 2003

[2] Kurt S, Wolfgang R, Oskar P. Formation of paint surface on different surface structure of steel sheet. Iron and Steel Engineer. 1997;**74**(3):43-49

[3] Ryk G, Kligerman Y, Etson I. Experimental investigation of laser surface texturing for reciprocating automotive components. Tribology Transactions. 2002;**45**(4):444-449

[4] Temmler A, Willenborg E, Wissenbach K. Design surface by laser remelting. Physics Procedia. 2011;**12**(1): 419-430

[5] Lugomer S. Laser Technology-Laser Driven Processes. Englewood Cliffs, NJ, USA: Prentice Hall Inc; 1990. pp. 419-439

[6] Duley WW. Laser Processing and Analysis of Materials. New York and London: Plenum Press; 1983

[7] Nüsser C, Wehrmann I, Willenborg E. Influence of intensity distribution and pulse duration on laser mico polishing. Physics Procedia. 2011; **12**(1):462-471

[8] Galarneau P, Levesque M, Beaulieu R, et al. Laser micromachining of optical fibre: An instrumentation enabler. Physics Procedia. 2010;**5**(1): 477-482

[9] Murthy Peri MD, Varghese I, Cetinkaya C. Laser cleaning for removal of nano/micro-scale particles and film contamination. In: Developments in Surface Contamination and Cleaning. Methods for Removal of Particle Contaminants. Elsevier, UK: William Andrew; 2011. pp. 63-122

[10] Guo KW. Effect of polishing parameters on morphology of DF2 (AISI-O1) steel surface polished by Nd: YAG laser. Surface Engineering. 2009; **25**(3):187-195

[11] Guo W. Effect of irradiation parameters on morphology of polishing DF2 (AISI-O1) surface by Nd:YAG laser. Research Letters in Materials Science. 2007;**51316**:1-5. DOI: 10.1155/2007/ 51316

[12] Shen N, Matthews MJ, Fair JE, et al. Laser smoothing of sub-micron grooves in hydroxyl-rich fused silica. Applied Surface Science. 2010;**256**(12): 4031-4037

[13] Janna WS. Engineering Heat Transfer. Boston: PWS Engineering; 1986

[14] Jastrzebski ZD. The Nature and Properties of Engineering Materials. 3rd ed. New York: John Wiley & Sons; 1987